Bulletin of Geophysics and Oceanography Vol. XX, n. X, pp. XXX-XXX; Xxxxx 20xx
DOI 10.4430/bgo00478

Analysis of short-term Sentinel-1 data using the DInSAR method for monitoring displacement following the earthquakes of 6 and 20 February in Hatay city

S. Doğanalp[1], B. Coşkuner[2] and H.B. Makineci[1]

[1] *Geomatics Engineering Department, Konya Technical University, Selçuklu, Konya, Turkey*
[2] *Geological Engineering Department, Konya Technical University, Selçuklu, Konya, Turkey*

(Received: 27 December 2023; accepted: 20 September 2024; published online: 31 October 2024)

ABSTRACT The Eastern Anatolia Fault Zone (EAFZ) has caused destructive earthquakes. Kahramanmaraş and Hatay, located on the EAFZ, were hit by devastating earthquakes with magnitudes of 7.7, 7.6, and 6.3, respectively, in February 2023. A tectonic chain of disasters was seen in Hatay in a short time, first on 6 February 2023, with earthquakes centred in Kahramanmaraş and the subsequent intense earthquake series, and lastly on 20 February 2023, with the Hatay earthquake centred in the Yayladağ district. The lithological characteristics of the units in the region increased the destructive effects of the earthquakes. In addition, the location of the study area, where the EAFZ and the Death Sea Fault Zone are close to each other, increases the importance of research. This study aims to monitor the ground displacements caused by the earthquakes in Hatay. Sentinel-1A Synthetic Aperture Radar data was acquired on 29 January, and 10 and 22 February, and the Differential Interferometry Synthetic Aperture Radar method was applied. In addition, the elevation change was determined by using two-month global navigation satellite system data from the Continuously Operating Reference Station points (HAT2 and ONIY) in the study area. Thus, considering regional tectonics, ground movements resulting from the earthquakes on 6 and 20 February were identified and examined using geologic, geodesic, and remote sensing techniques.

Key words: Death Sea Fault Zone, DInSAR, East Anatolian Fault Zone, 6 February 2023 Pazarcık (Kahramanmaraş) earthquakes, 20 February 2023 Hatay (Yayladağ) earthquake.

1. Introduction

With the collision of the Anatolian and Arabian plates along the Bitlis - Zagros suture zone (Şengör, 1980), Turkey, which contains many tectonic fragments, has recently entered a new tectonic period called neotectonic. As a result of this collision, the Eastern Anatolia region acquired fold and thrust structure and became shorter and thicker (Fig. 1). Due to the increasing crustal thickness, the Anatolian plate moved westwards towards the eastern Mediterranean along the right-lateral strike-slip North Anatolian Fault Zone (NAFZ) and along the left-lateral strike-slip Eastern Anatolian Fault Zone (EAFZ) under the lithostatic pressure (Şengör, 1980; McClusky *et al*., 2000). This movement was blocked by the Greek shear zone and, as a result, the Aegean region was under an east-western compressive and north-southern extensional tectonic

regime, leading to the formation of graben structures in the east-western direction (Fig. 2). The continuous northward movement of the Arabian plate caused the formation of the left-lateral strike-slip Ölüdeniz Fault Zone between the Arabian and African plates. As a result of the collision of the Anatolian and Arabian plates, Turkey was divided into four main neotectonic regions, namely the East Anatolian Contractional Province (EACP), Central Anatolian "OVA" Province (CAOP), and West Anatolian Extensional Province (WAEP), and North Anatolian Province (NAP) (Şengör, 1980; Şengör *et al*., 1985).

In the study area in which the EAFZ and the Dead Sea Fault Zone (DSFZ) are close to each other, earthquakes occurred in Pazarcık (Kahramanmaraş) on 6 February 2023 and Hatay (Yayladağ) on 20 February 2023, with magnitudes of 7.7 and 6.3, respectively. These devastating earthquakes caused great damage in 11 different cities. As a result of the earthquakes, many geological, geotechnical, and geodesic studies were carried out (Abdelmeguid *et al*., 2023; Akıncı and Ünlügenç, 2023; Aksoy *et al*., 2023; Altunsu *et al*., 2023; Baser *et al*., 2023; Bulbul *et al*., 2023; Caglayan *et al*., 2023; Fusco *et al*., 2023; Görüm *et al*., 2023; Harzali *et al*., 2023; Karabacak *et al*., 2023; Kim and Han, 2023; Kürçer *et al*., 2023; Kwiatek *et al*., 2023; Liu *et al*., 2023; Zhang Y. *et al*., 2023; Kobayashi *et al*., 2024) and the deformation structures were investigated in detail. The earthquake that occurred on 6 February 2023 in Pazarcık caused a 400-kilometre long deformation zone. The amount of displacement at 410 points along this zone was measured by field studies and displacement was determined to be 7.2±0.1 m and 3.9±0.1 m in the Pazarcık segment and Narlı segment, respectively, with a total left lateral displacement measured of 11.1±0.1 m (Kürçer *et al*., 2023). The 20 February 2023 earthquake in Hatay was recorded on a normal-component left-lateral strike-slip fault (Kürçer *et al*., 2023).

Differential Interferometry Synthetic Aperture Radar (DInSAR) is a remote sensing method used to monitor and measure changes in the Earth's surface using high-resolution radar images (Ferretti *et al*., 2007; Fusco *et al*., 2023). DInSAR is widely used to identify and monitor surface deformations, especially in areas involved with ground subsidence, groundwater level changes, mining operations, or construction projects (Monterroso *et al*., 2018; Gupta *et al*., 2019; Ullo *et al*., 2019; Pawluszek-Filipiak and Borkowski, 2020; Xu *et al*., 2021; Rafiei *et al*., 2022; Kim and Han, 2023). Actually, it is widely preferred for high-accuracy monitoring of surface deformations using the DInSAR method and Synthetic Aperture Radar (SAR) data (Yagüe-Martínez *et al*., 2016; Gupta *et al*., 2019; Xu *et al*., 2021). Depending on the band type (e.g. C, L, or X) and spatial resolution (range and azimuth directions) of the SAR sensor, displacement detection can be made with millimetre precision (Makineci, 2023). DInSAR has also been used to determine the speed and direction of changes in the surface. This is especially important for determining and monitoring the effects of events such as earthquakes, volcanic eruptions, landslides, and floods (Gupta *et al*., 2019; Krishnakumar *et al*., 2021). In addition, the temporal resolution of the sensor and the perpendicular baseline directly affect the accuracy of the product obtained. Whether the data used is short-term or long-term is important in determining the amount of movement in the selected range (Sandron *et al*., 2023).

As part of the application scope, the data from two Continuously Operating Reference Stations in Turkey (CORS-TR) in the region (HAT2 and ONIY) were evaluated, and the positioning changes over two months were obtained. In recent years, web-based Global Navigation Satellite System (GNSS) positioning services have played an effective role in the evaluation of GNSS data (Basciftci and Bulbul, 2022; Erkoç and Doğan, 2023). Through these services, location information can be obtained at centimetre level by uploading data collected from a single receiver to the respective service (Yigit *et al*., 2022). Some of the most well-known services include CSRS-PPP, APPS,

GAPS, SCOUT, Magic-GNSS, and Trimble CenterPoint RTX. The Trimble CenterPoint RTX service, developed in 2011 and aiming to achieve centimetre-level accuracy using GNSS signals, stands out among these services (Alkan, 2019; Erol *et al*., 2020). Within the scope of the application, two-month data of two CORS-TR stations (HAT2 and ONIY) in the region were evaluated and the results were obtained.

This study aims to determine the ground deformations that occur in very large areas, which are almost impossible to detect by *in-situ* works by researchers after the February 2023 significant earthquakes, on the ground displacement map created with Sentinel-1 SAR Earth observation data. Considering the Amik Plain and Amanos Mountain massif, which cover a large part of the selected area, SAR data sets were preferred as descending orbits. Within the scope of this study, using the two-pass DInSAR method, which is a frequently used method in the literature, ground movement changes were monitored in displacement maps produced from three short-term and temporal baseline data for a total of 24 days. In order to ensure that the detection of surface deformations is not limited to remote sensing alone, the location information of two national GNSS points (ONIY and HAT2), enabling the detection of local movements, was taken from the database, and their displacements (horizontal and vertical), before and after the earthquake, were calculated. Then, a comparative analysis was conducted between the trends of local movements found on the displacement map obtained by the InSAR method and the data obtained from two CORS-TR stations, continuously performing measurements. Consequently, the ground movements determined from the displacement map obtained with the SAR data sets and ground movements seen at the CORS points were consistent for both earthquakes. As *in-situ* studies could not rapidly and accurately determine surface deformations over large areas affected by significant earthquakes, it is proven that surface deformations can be identified using displacement maps produced by SAR data sets. This study monitored the 6 and 20 February earthquakes in Hatay city with DInSAR method surface deformation maps using short-term Sentinel-1 SAR data, finding consistent movement with CORS-TR data and identifying approximately one metre of surface deformation on 6 February and 15 cm on 20 February.

1.1. Geological settings

The basement of the study area is formed by Pre-Cambrian quartzite and metaclastic alternation exposed west of Hassa. This Pre-Cambrian unit is conformably overlain by Paleozoic quartzite, marble, calc-shist, and metaclastic alternation. These basement Paleozoic units, which surface in the north of the study area, are unconformably overlain by Mesozoic-aged limestone, dolomite, and cherty limestone. The Mesozoic units are tectonically overlain by the Cretaceous ophiolitic rocks, which consist of serpentine, diabase, and gabbro. The ophiolitic succession outcrops, in the SW-S of the study area, are unconformably overlain by Eocene - Pliocene limestone, claystone and terrestrial clastic alternation. All the above-mentioned units are unconformably overlain by Quaternary aged alluvium, which outcrops in a wide area around the Amik plain (Fig. 1).

1.2. Regional tectonic

The study area is located at the intersection of the African, Anatolian, and Arabian plates in terms of tectonic position. The EAFZ and DSFZ constitute the important tectonic structures in the studied area. The EAFZ, which was first identified by Allen (1969), is shown with small-scale

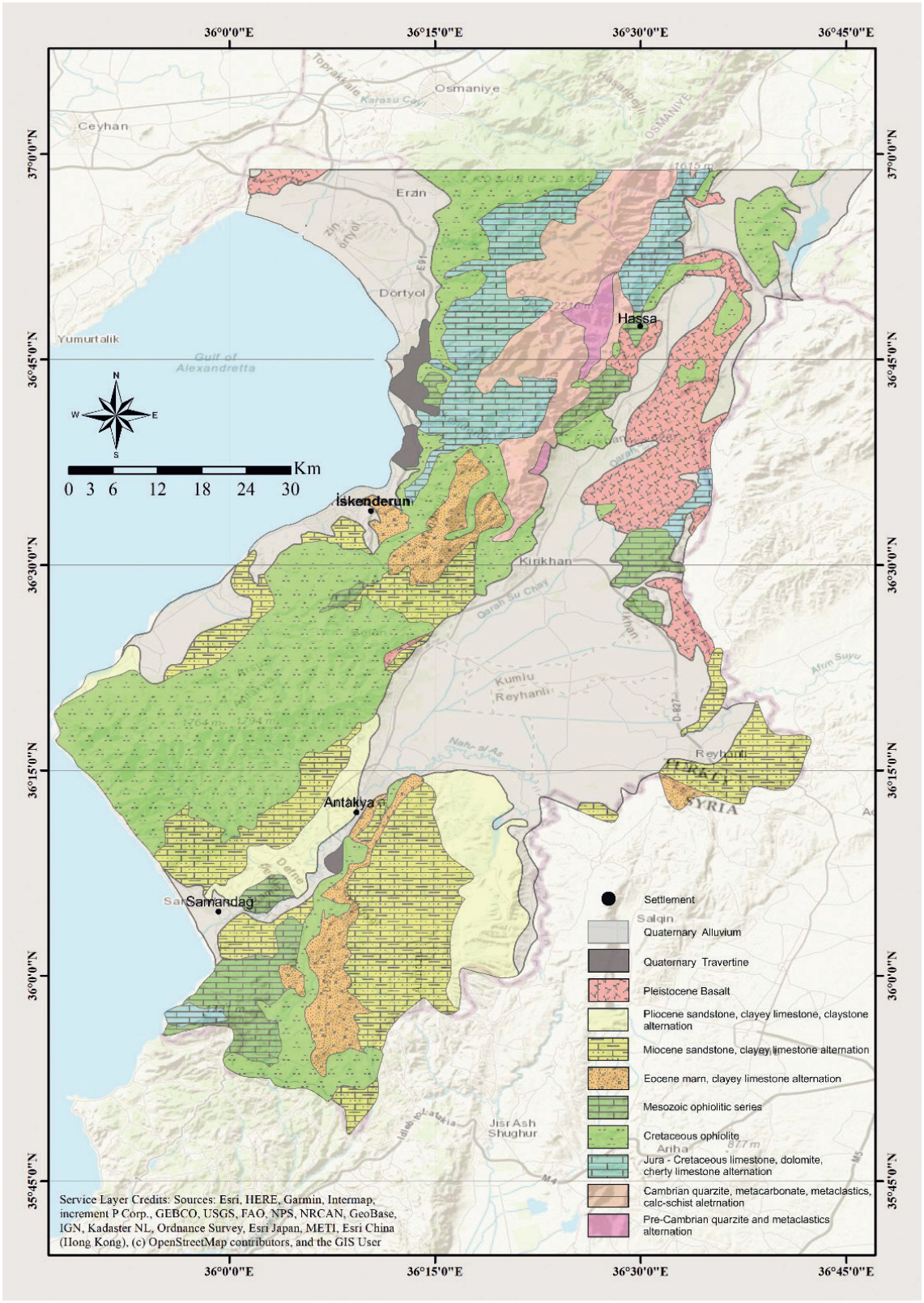

Fig. 1 - Geological map of study area.

schematic maps. On 22 May 1971, as a result of the Bingöl earthquake, the EAFZ was mapped by Arpat and Şaroğlu (1972) using various methods. The 600-kilometre long EAFZ, extending as a boundary between the Anatolian and Arabian plates, starts from the Karlıova (Bingöl) triple junction point and connects to the Cyprus arc towards the SW. The slip rate of the left-lateral strike-slip fault is approximately 6 to 10 mm/year (McClusky *et al*., 2000; Reilinger *et al*., 2006). The EAFZ, mainly divided into two different segments which are the main branch and the northern branch, was divided into different segments by Kürçer *et al*. (2023). The main branch of the EAFZ is divided into the Karlıova, Ilıca, Palu, Pütürge, Erkenek, Pazarcık, Amanos, Serinyol, and Antakya segments from NE to SW. The study area within the main branch includes a part of the Amanos segment of the EAFZ, which is 130 km long and trending N35˚E, the Serinyol segment, which is 19 km long and trending N20˚E, and the Antakya segment, which is 45 km long and trending N35˚E (Fig. 2) (Kürçer *et al*., 2023).

When the historical tectonic activities in the region were investigated, they revealed that a very destructive earthquake occurred in 69 B.C. and was felt in Cyprus and Magossa and affected Antakya and some cities in Syria (Andreasyan, 1964, 1973; Andreasyan and Dulaurier, 1987). Many destructive earthquakes have occurred in the study area in the historical period (149 B.C.-1875) (Soysal *et al*., 1981). Until 6 February 2023, in the instrumental period, 56 earthquakes were recorded in the studied area with a magnitude greater than 4, of which 49 with a magnitude less than 5, and seven with a magnitude between 5 and 6. Between 5 February 2023 and 21 February 2023, 51 earthquakes were recorded in the study area with a magnitude greater than 4, of which 47 were smaller than 5, three were smaller than 6, and one with 6.4 magnitude (Fig. 3). All earthquakes occurred at shallow depths, and the maximum depth was 21.74 km. According to the focal mechanisms, it is observed that the study area contains strike-slip, oblique, and normal faults (AFAD, 2023). The studies carried out by Kürçer *et al*. (2023) determined an average displacement of 379 ± 14 cm in the left direction due to the 7.7 magnitude earthquake that occurred on 6 February 2023 on the Pazarcık segment.

2. Material and methods

2.1. Study area

The Amik Plain and Nur Mountains, situated in the centre of the crater area inside the boundaries of Hatay province, encircle the study area, that has a thick layer of alluvial soil with great agricultural potential (Fig. 1). Until recently, in the Amik Plain, there once was a lake known as Amik Lake, fed by the Asi River, Karasu, and Afrin Streams. However, the lake, which was 16 km long and 10 km wide, and a portion of the 310 km^2 surrounding it, have dried up, leaving the area to be replaced by highly productive agricultural land (Çalışkan, 2008).

2.2. Two-pass differential Interferometry

The displacement monitoring procedure uses the two-pass DInSAR method and Sentinel Application Platform (SNAP) software. Typically, this process uses short-term SAR data to determine ground deformations (Ferretti *et al*., 2007; Yagüe-Martínez *et al*., 2016; Gupta *et al*., 2019; Small and Schubert, 2019; Krishnakumar *et al*., 2021). The following are the steps involved in processing Sentinel-1 TOPS InSAR data:

i. S-1 TOPSAR split;

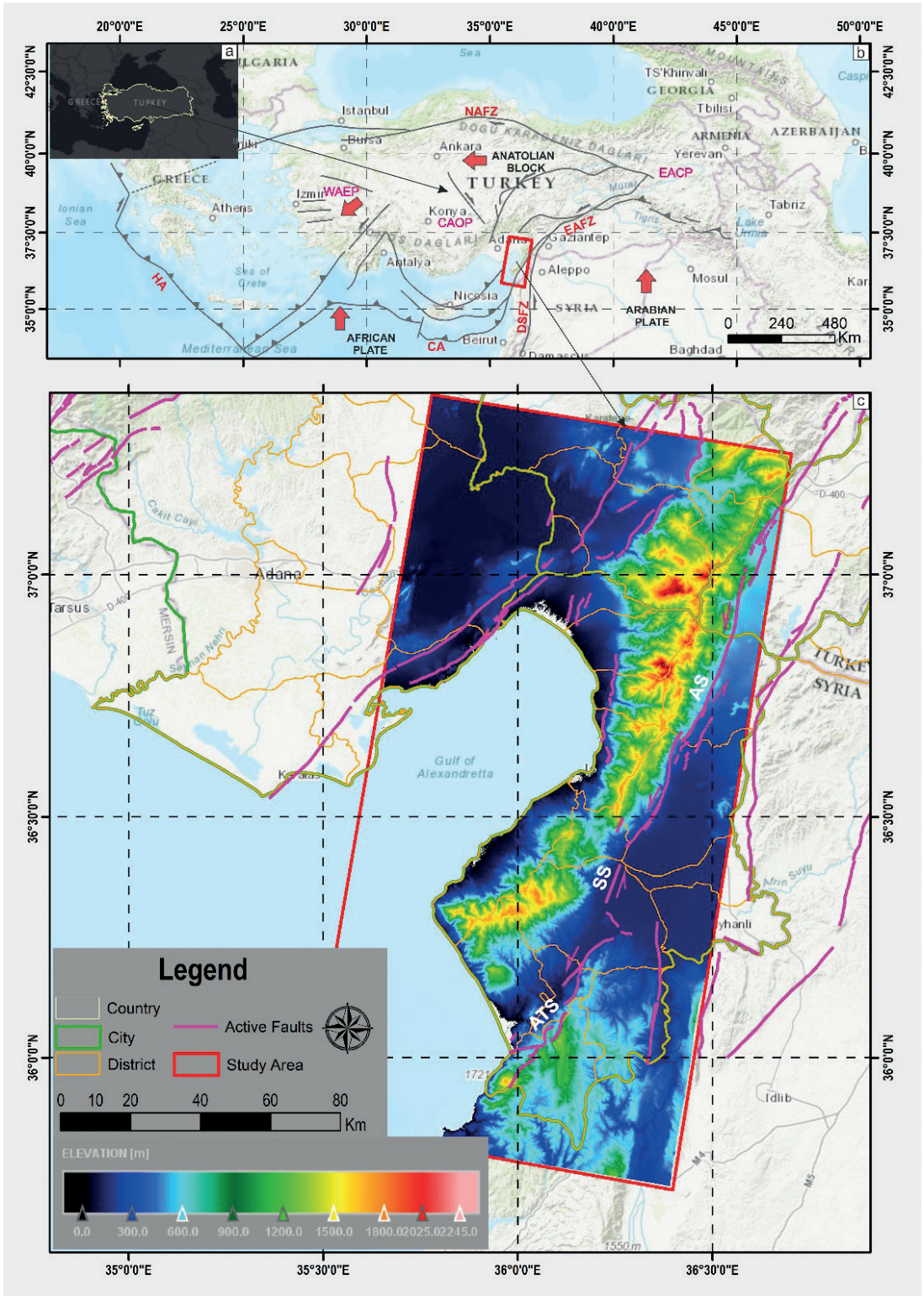

Fig. 2 - a) Location of Turkey; b) neotectonic structures and provinces of Turkey; DSFZ, EAFZ, NAFZ, Helenic Arc (HA), Cyprus Arc (CA), EACP, CAOP, WAEP (Şengör, 1980; Şengör *et al*., 1985); c) active faults and the Amanos , Serinyol, and Antakya segments of the EAFZ (Emre *et al*., 2013; Kürçer *et al*., 2023).

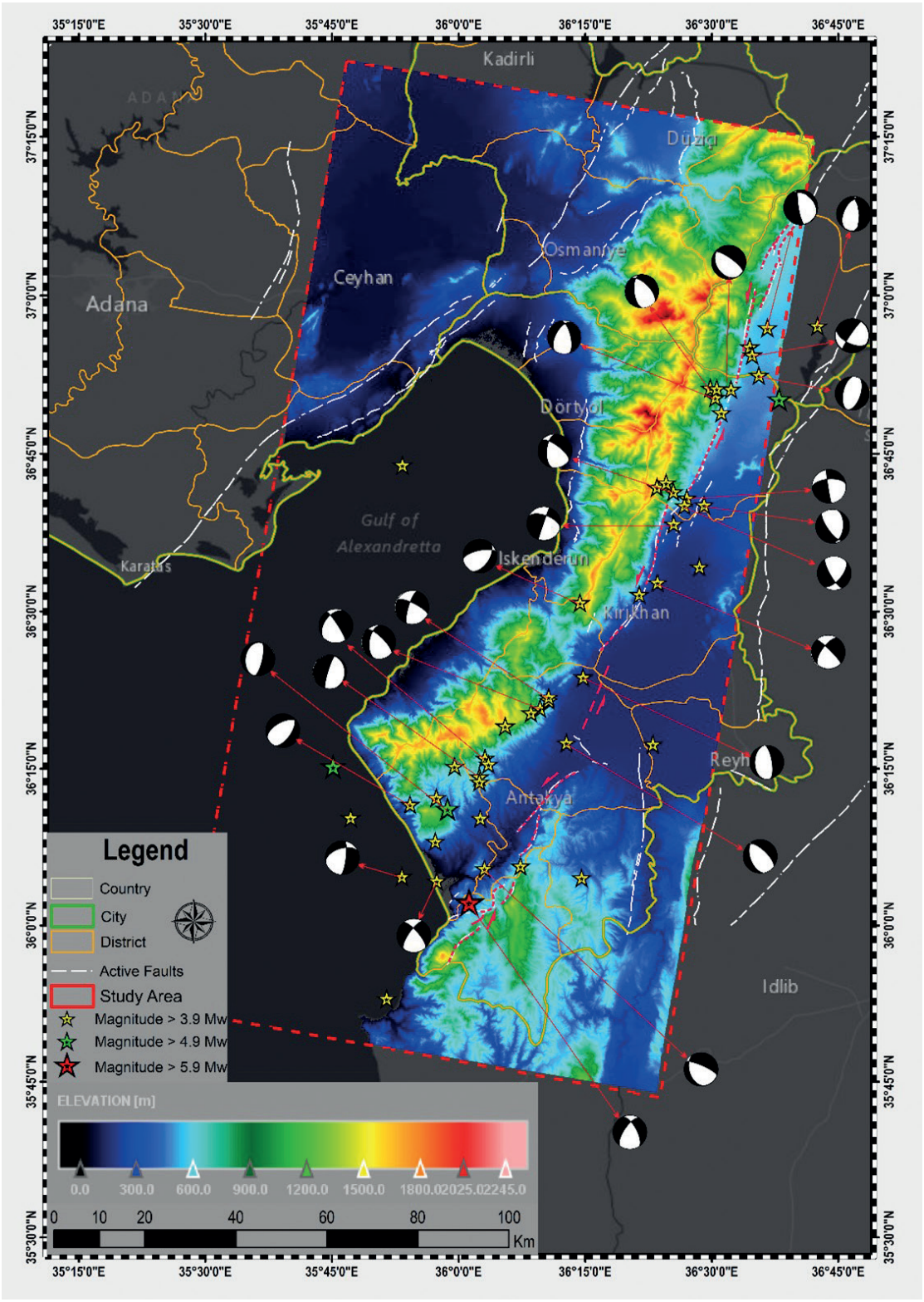

Fig. 3 - Earthquakes with a magnitude greater than 4 and their focal mechanism solutions that occurred between 6 February 2023 and 21 February 2023 in the study area (AFAD, 2023).

ii. orbit file application;
iii. S-1 back geocoding: the orbits of the two products and a Digital Elevation Model (DEM) are used to co-register two S-1 SLC split products (reference and secondary) onto the same sub-swath products. The secondary image is initially processed through deramp and demodulation before being subjected to truncated-sinc interpolation in order to resample it into the reference frame (Gupta *et al*., 2019; Small and Schubert, 2019; Sarmin *et al*., 2020;);
iv. S-1 enhanced spectral diversity (ESD) implementation: after TOPS co-registration, the Network Enhanced Spectral Diversity process is implemented in the data (Fattahi *et al*., 2017). Constructing a network (graph) of images and, then, solving an optimisation problem accomplishes the joint co-registration of a Sentinel-1 stack. By considering the offsets of several reference and secondary pairs, the ESD process computes fixed azimuth and range offsets (for each data) concerning reference data (Yagüe-Martínez *et al*., 2016);
v. interferogram creation;
vi. S-1 TOPSAR deburst;
vii. estimation and removal of the topographic phase;
viii. multilooking: a typical SAR image has intrinsic speckle noise and appears speckled. To lessen the natural speckled appearance, multiple images are randomly blended together to appear as though they represent various aspects of the same scene. Additionally, an application product with a nominal image pixel size can also be created using multilook processing (Small and Schubert, 2019);
ix. phase filtering: a preprocessing method that improves phase unwrapping accuracy (PU) and drastically lowers residues in the subsequent step. Goldstein and Werner's nonlinear adaptive algorithm serves as the basis for the method used in this operator (Goldstein and Werner, 1998);
x. unwrapping: unambiguous phase data can be recovered from a 2D array of phase values, known to module 2πr, through a technique called two-dimensional PU. SNAPHU implements the Chen and Zebker (2001) statistical-cost, network-flow algorithm for PU. In this research, the interferograms were unwrapped by applying the minimum cost flow algorithm in SNAPHU software (Chen and Zebker, 2001);
xi. phase-to-displacement implementation: the following additive phase term [Eq. (1)], independent from baseline, appears in the interferometric phase if some of the ground-based point scatterers slightly shift their relative positions in the time interval between two SAR observations (i.e. subsidence, landslide, earthquake, etc.) (Ferretti *et al*., 2007):

$$\Delta\emptyset_d = -\frac{4\pi}{\lambda}d \quad (1)$$

where the relative scatterer displacement, *d*, is projected on the slant range direction and is the transmitted wavelength. The three contributions to the interferometric phase variation are as follows:

I. a phase variation, known as a horizontal reference plane, that is proportionate to the relative terrain altitude;
II. a phase variation in accordance with the point target slant range differences;
III. a phase variation that varies in accordance with the relative scatterer displacement.

If a DEM is available, the first phase term (the altitude contribution) can be subtracted

from the interferometric phase. Topographic phase removal is the term for this procedure. An additional method for computing and subtracting the second phase term from the interferometric phase is to use precise orbital data. The process is known as flat-Earth phase removal or interferogram flattening. The two above-mentioned procedures are followed by the creation of a phase map that is solely proportionate to the relative displacement of the terrain, which can be calculated with (Ferretti *et al*., 2007):

$$d = -\frac{\lambda}{4\pi}\Delta\emptyset_d; \quad (2)$$

xii. range doppler terrain correction;
xiii. coherence mask.

2.2.1. Monitoring of surface deformation using InSAR with Sentinel-1 IW data

When converting unwrapped phases into displacement values, the preference is to use the following Eq. (3) to convert PU to vertical displacement in the general procedure rather than in the line-of-sight (LOS) direction:

$$d = -\frac{\lambda \times \phi}{-4\pi \times cos\theta inc}. \quad (3)$$

The descending orbit incident angle (θ_{inc}) range is essential for the ground deformations that are attempted to be detected in the study area. In particular, it is used as a variable from the tie-point grids to avoid errors resulting from manually-determined incident angles. The units of the results (i.e. the wavelengths) will be in centimetres (Table 1). The values show the elevation difference towards the sensor, which means variation along the LOS. In the old versions of the software used, users were attempting to perform these calculations manually and encountered incorrect results. For the latest versions, the SNAP software can derive a vertical displacement map directly from the "Phase-to-displacement implementation" results.

2.3. Data used in the study

2.3.1. Remote sensing data

Sentinel-1 SAR satellite data is free Earth observation data with a 30-metre spatial resolution that the European Space Agency (ESA) makes available free of charge to users. Data with a resolution of 12.33 m × 3.29 m in azimuth and range directions, respectively, were acquired by the descending orbit. Since deformation could not be determined with single SAR data, two reference-secondary pairs were created with three descending orbit satellite data to perform the two-pass DInSAR method. The optimal reference data was determined by performing an InSAR stack overview and reference selection. The data downloaded as a single-look complex (SLC) consists of three sub-swaths. Each sub-swath is divided into nine frames. IW3 VV from split SLC data is used in the study. The characteristics of the data used in the analysis are presented in Table 1. The least amount of deviation from the perpendicular baseline characterises the reference data selection. The optimisation of the expected stack coherence of the interferometric stack is the goal of the reference selection. The reference, considered optimal, supports quality evaluation by suggesting the enhanced visual comprehension of the interferograms.

Table 1 - Specifications of Sentinel-1 data used in the study.

Acquisition date	Type of data	Reference/ secondary	Track	Orbit	Perpendicular baseline (m)	Temporal baseline (days)	Modelled coherence (expected-%)	Azimuth x range resolution (m)	Band type
29 Jan. 2023	SLC	Secondary	21	46993	104.33	-12	0.90	12.3 × 3.3	C
10 Feb. 2023	SLC	Reference	21	47168	0.00	0	1.00	12.3 × 3.3	C
22 Feb. 2023	SLC	Secondary	21	47343	-65.09	12	0.93	12.3 × 3.3	C

The SAR data acquisition geometry is shown in Eq. (4). Initially, after collecting omega (Ω), phi (Φ), and lambda (λ) information from the reference (master) data topography, secondary (slave) data is taken. The change between master and slave data shows the amount of topography that is deformed in total (Δ_d):

$$\begin{aligned} &\text{master data:} && \Delta_M = \Omega_M + \Phi_M + \lambda_M \\ &\text{slave data:} && \Delta_S = \Omega_S + \Phi_S + \lambda_S \\ &\text{deformation of topography:} && \Delta_d = \Delta_M - \Delta_S. \end{aligned} \tag{4}$$

2.3.2. CORS-TR (TUSAGA) points and trimble-RTX service

The CORS-TR system is a network consisting of 158 fixed GNSS stations, including four stations in Cyprus, continuously measuring, i.e. 24 hours a day, seven days a week. The system collects data from all stations at one-second intervals for 24 hours and sends these data to the control and analysis central stations via the Internet (Yildirim *et al*., 2013). The GNSS data received is processed in control and analysis centres, and correction data, enabling location determination, are calculated and published for users. Thanks to the real-time data collected by the system, in addition to specific studies (such as meteorological applications, tectonic movements, and modelling of the ionosphere layer), many cartography applications (such as geographical information systems and infrastructure services) can be easily carried out (General Directorate of Mapping, 2018a).

In the Trimble CenterPoint RTX service, GNSS data collected from 120 ground stations scattered worldwide are transmitted to the control centre via the Internet. Thanks to the data transmitted to the control centre, atmospheric data, Earth rotation parameters, and other correction data are determined, after which precise satellite orbit and clock information are obtained. Once the correction data have been determined, the satellite sensitive orbit and time information are obtained (Zhang F. *et al*., 2013; Brandl *et al*., 2014; Yigit *et al*., 2022). In order to use the service, it is necessary to create an online registration. After registration, observation files can be uploaded and results obtained. Observation files should be dual frequency, containing pseudo range and carrier phase observations (L1 and L2), observations should last at least 60 minutes in order to obtain optimal results, data files should be static, and file lengths should not exceed 24 hours. The data formats, used in the evaluation, support standard formats (RINEX 2 and RINEX 3) as well as Trimble special formats (DAT, T01, T02, T04, etc.). If the data files do not meet the above-mentioned conditions, the service cannot evaluate them (Trimble-RTX, 2021).

Trimble-RTX, an online process service, aims to achieve centimetre-level accuracy using GNSS signals with proprietary algorithms and online calculations. The service, which offered

approximately 4 cm of horizontal accuracy until 6 August 2018, can now provide 2 cm of horizontal and 5 cm of vertical position accuracy (Alkan, 2019; Alkan *et al*., 2020). Position calculations are performed at the ITRF2008 datum 2005.0 epoch for data sets collected before 23 March 2017 and at the measurement moment epoch in the ITRF2014 datum for data sets collected after 23 March 2017 (Trimble-RTX, 2021). However, users can also choose a different coordinate system or tectonic plate for location calculations. Additionally, if the tectonic plate is not selected (autodetect), the service automatically detects the tectonic plate. After selecting the coordinate system and tectonic plate to evaluate the data files, the observation files are uploaded, and e-mail information is entered to receive the results. Once the service has pre-checked all the information entered, it sends the results to the specified e-mail address within approximately two minutes.

Within the scope of the application, two months of data from two CORS-TR stations (HAT2 and ONIY) in the region were evaluated, and the relevant results were obtained. According to the decision taken, 1-second data of the CORS-TR stations, located in the earthquake region on dates when an earthquake of magnitude 5 or higher occurred in Turkey, are published free of charge (General Directorate of Mapping, 2018b). The data of the HAT2 and ONIY stations used in the study were downloaded and, then, converted into 30-second data, and the location information of the stations was obtained from the Trimble CenterPoint RTX service, one of the web-based GNSS positioning services.

2.4. General workflow of the study

SNAP, a free-of-charge and open-source software produced by ESA, is used to process and analyse Sentinel missions Earth observation data (Sonkar *et al.*, 2023). After completing interferometry on Sentinel-1 SAR data, using SNAP software and creating a displacement map, terrain correction and export are performed. Integrated maps are produced by creating simultaneously TUSAGA points, active faults, and earthquakes in Geographic Information System software. These processes and the general workflow are presented in Fig. 4.

3. Results and discussions

The results obtained in this study clearly show the presence of deformations both in the vertical and in the horizontal direction. The vertical movements, which are generally associated with dip-slip and oblique faults, also occur in areas where the strike-slip faults bend or jump. The results obtained in this study clearly show the presence of deformations in the vertical direction. The vertical movements, which are generally associated with dip-slip and oblique faults, also occur in areas where the strike-slip faults bend or jump. The focal mechanism solutions of the earthquakes in the region show that earthquakes occurred due to normal, oblique, and strike-slip faults (Fig. 3). As a result of these, deformation structures developed not only laterally but also vertically in the study area. In order to correctly explain the vertical deformations, it is important to evaluate the deformed areas together with the faults in the region.

When the ground displacement map was analysed, through images before and after the Pazarcık earthquake, it was found that areas were uplifted by 44 cm and subsided by 62 cm in the region (Fig. 5). According to the results obtained, after the 7.7 magnitude Pazarcık earthquake of 6 February, a vertical movement of approximately 1 m occurred in the region. One of the reasons for these vertical movements in the region is the presence of compressional and extensional

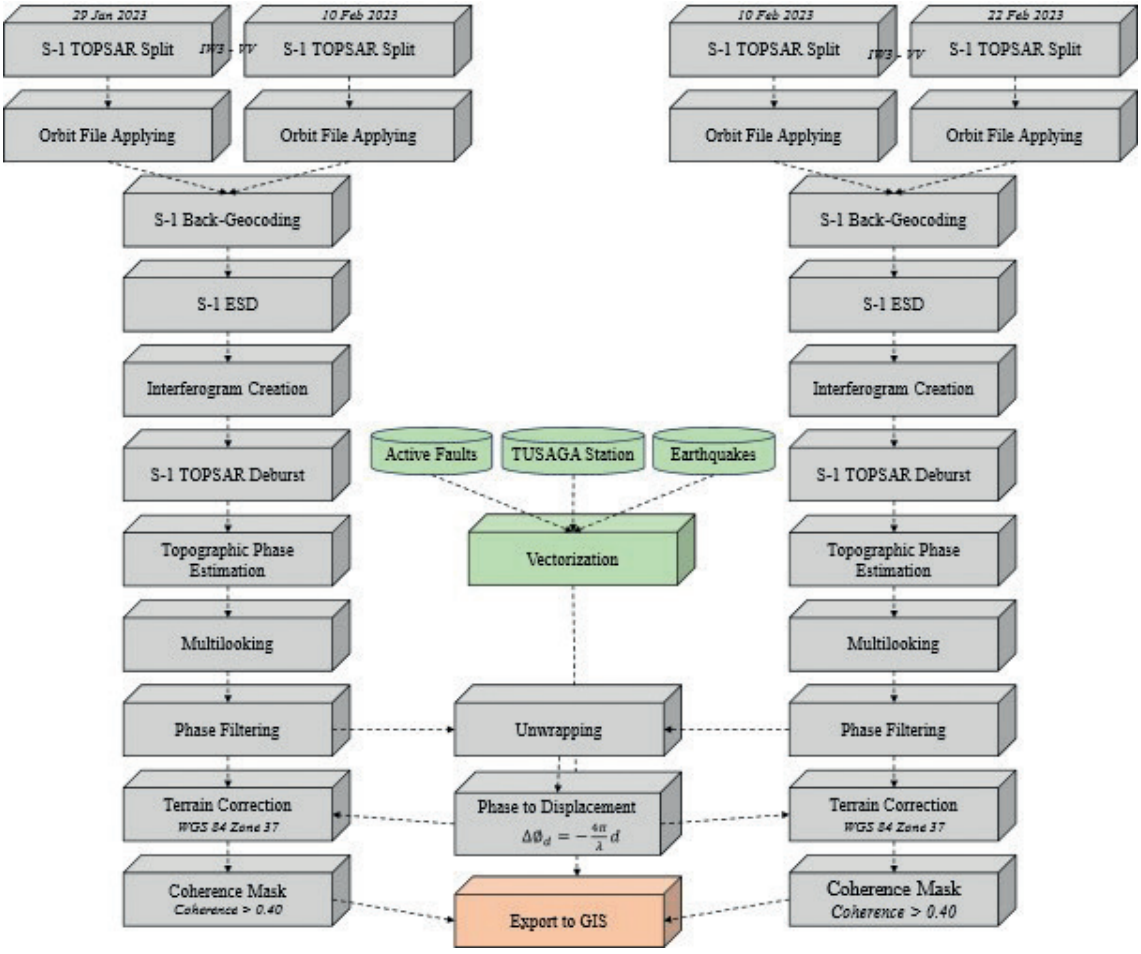

Fig. 4 - The workflow of the study.

areas, which developed due to the bending of the fault. The paired bends in the area of the Yuvalı and Taşoluk villages, north of Kırıkhan, are a good example of this situation (Fig. 5). As a result of the bending, the section in the Yuvalı village in the compressional area was uplifted by 40 cm, while the area in the Taşoluk village in the extensional area subsided by 60 cm (Fig. 5a), and movement occurred in the vertical direction for totally 1 m. Another result obtained from the analyses based on the displacement map is the vertical deformation observed on the Serinyol segment mapped by Kürçer *et al*. (2023). The subsiding and uplifting zones are sharply separated along the segment in this deformation area. The mountainous area in the WNW of this fault line was observed to have subsided by approximately 30 cm, while the basin area in the SE part of the fault line was uplifted by 44 cm. This vertical deformation structure indicates that the Serinyol segment may have an oblique fault character. The focal mechanism solution of the earthquake confirms this finding.

When examining the displacement map of the 20 February 2023 Hatay earthquake of magnitude 6.3, which occurred on the left lateral strike-slip fault with normal components, a 15-centimetre subsidence can be observed in the Antakya region (Fig. 6a). The normal fault component confirms this vertical movement (Fig. 6a). Also, when the obtained maps are analysed, the coastal region, located in SW Antakya and around Iskenderun, is observed

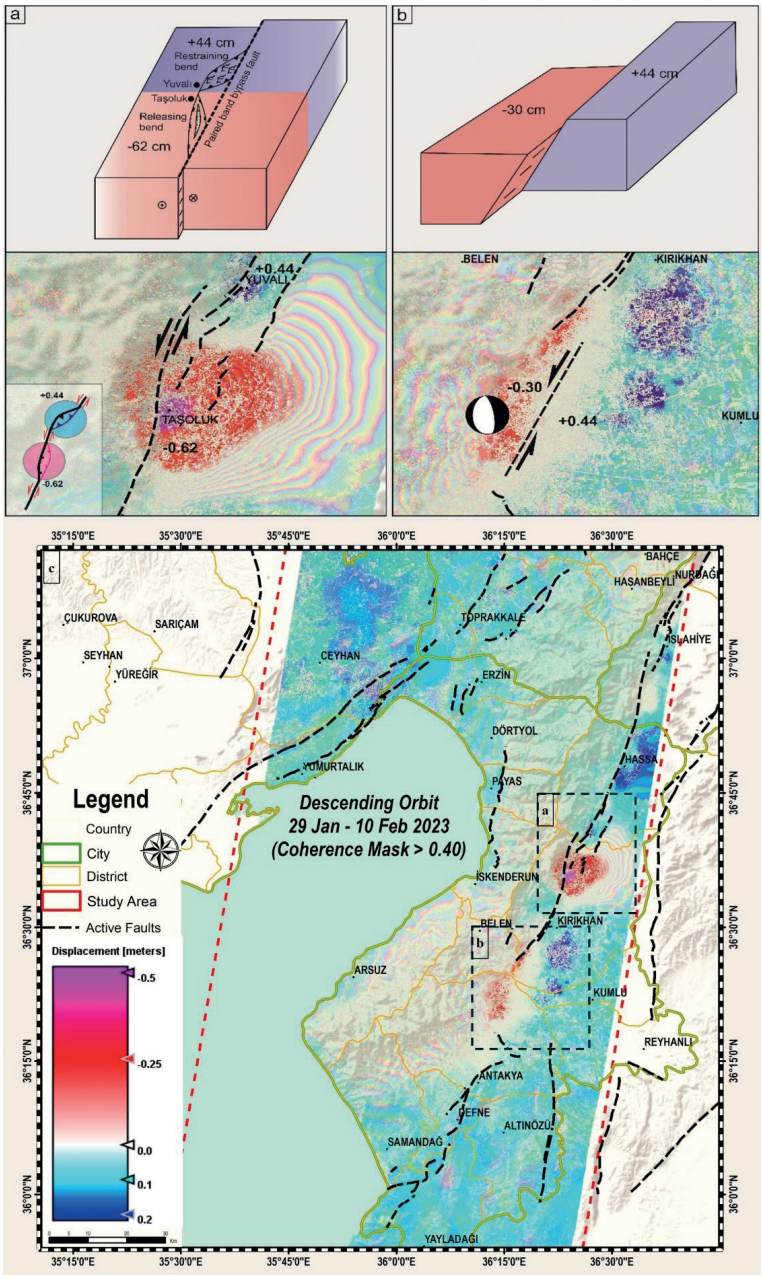

Fig. 5 - Map showing the area with an approximately 1-metre ground displacement due to paired bends in the study area (a); the region with a ground displacement of approximately 70 cm on the Serinyol segment (b); 29 January 2023 - 10 February 2023 ground movement map (c).

to have an approximate 12-centimetre subsidence (Figs. 6a and 6b). The rising sea level and inundation in the Iskenderun region confirm the vertical deformation. In addition, the deformations occurring on the steep coasts in SW Antakya are assumed to be related to the mass movements (Görüm *et al*., 2023) observed in the region. When the 6 February Pazarcık earthquake displacement map is examined, no deformation is observed on the Antakya coastline (Fig. 5). This indicates that the mass movements in the region may be related to the 20 February 2023 Hatay earthquake.

Interferograms, with coloured structures called fringes, produced with the InSAR technique, show deformation occurring at any point in the ground. They represent spatial ground movements

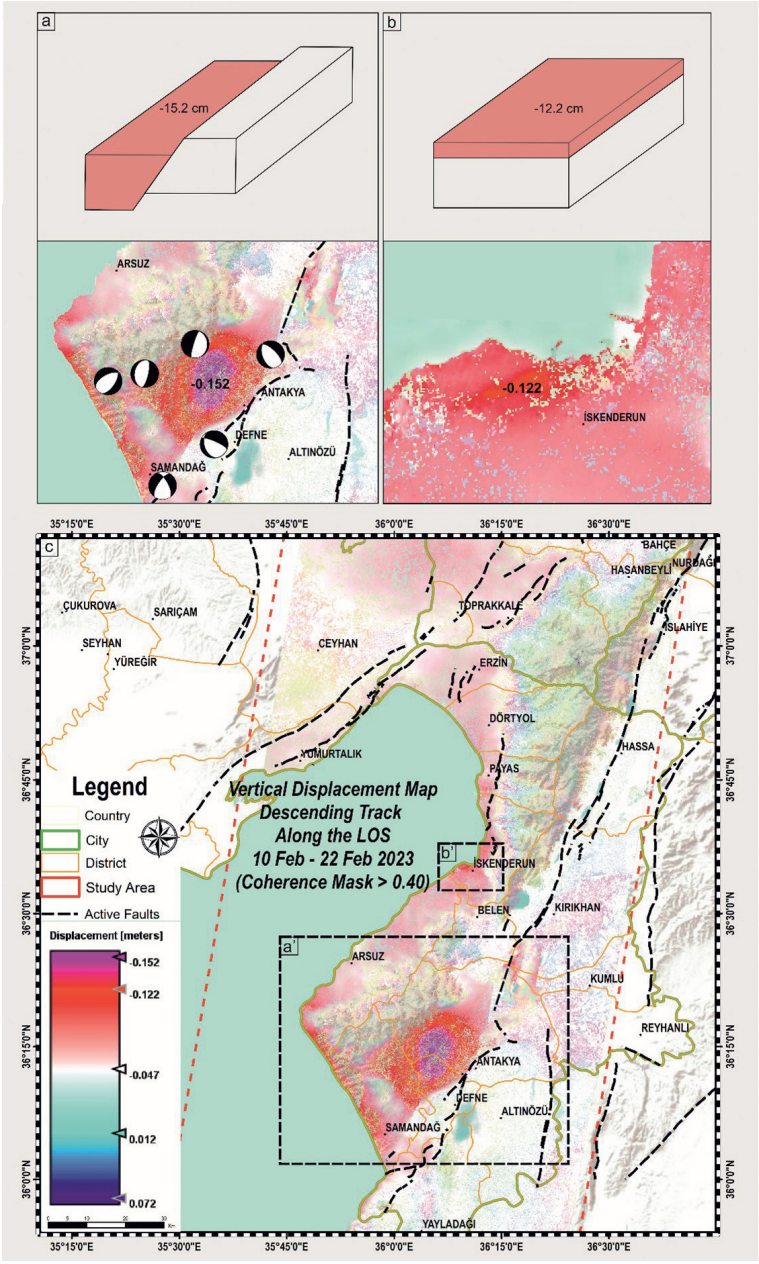

Fig. 6 - Map showing an approximately 15-centimetre vertical deformation and earthquake focal mechanisms in and around Antakya (a); 12-centimetre vertical deformation map in the Iskenderun region (b); 10 February 2023 - 22 February 2023 ground movement map (c).

by decreasing or increasing the distance from one fringe to the other (between -π and +π). As clearly shown in Fig. 5a, ground movement along the fault was determined in the Taşoluk rural area. Taşoluk and Yuvalı rural areas moved in opposite directions, 44 cm on one side and 62 cm on the other.

Within the scope of the application, two-month data [i.e. between 01 January 2023 (DOY: 1) and 28 February 2023 (DOY: 59)] of the Hatay (HAT2) and Osmaniye (ONIY) CORS-TR stations, which are located in the study region, were estimated by using the Trimble-RTX service. During the estimation step, data gaps were determined for the HAT2 station. This was due to the station becoming dysfunctional between 6 February 2023 (DOY: 37) and 17 February 2023 (DOY: 48)

when the earthquakes were active. Therefore, data between DOY: 38–47 could not be processed at the HAT2 station. Another data loss at the HAT2 station was due to the absence of L2 frequency in the observation file for DOY: 15 and, consequently, the Trimble-RTX service could not process the data. At the ONIY station, all data have been estimated, and show no data loss.

A summary of the results obtained for station HAT2 is shown in Fig. 7. Upon examining Fig. 7, it is clear that in the first earthquake (6 February-DOY: 37), the total number of GPS and GLONASS (Global Navigation Satellite System) satellites decreased from 50 to 20. Despite this, the HAT2 station, a testament to its robustness, started receiving data again during the second earthquake (20 February-DOY: 51), presenting a slightly more stable image. In addition, upon examining the ellipsoidal height change of the station, it can be said that it fluctuated a few centimetres until the moment of the first earthquake but maintained its general trend. The station height is observed to start to decrease five days before the earthquake. Since data from the station could not be obtained afterwards, the change could not be monitored precisely until approximately the moment of the second earthquake. The data taken three days before the second earthquake shows that the station suddenly rose after the 6 February earthquakes. This movement corresponds to an approximately 4-centimetre decrease, followed by an 8-centimetre increase. After the 20 February earthquake, the station started to decline again and, then, followed a fluctuating course due to the activity in the region.

Similarly, if the results of the ONIY station (Fig. 8) are examined, they show that the station had a stable image until the occurrence of the 6 February earthquakes, but on the day of the earthquake, the total number of satellites decreased from 50 to 20, the number of observations decreased from 3,000 to 450, and the standard deviation (StD) value increased. If these parameters are examined for the moment of the 20 February earthquake, it can be said that the station remained more stable and maintained its general trend. Similarly to the HAT2 station, the ellipsoidal height changes at the ONIY station maintained their average trend until the first earthquake, entered a decreasing trend five days before the earthquake, and gradually increased

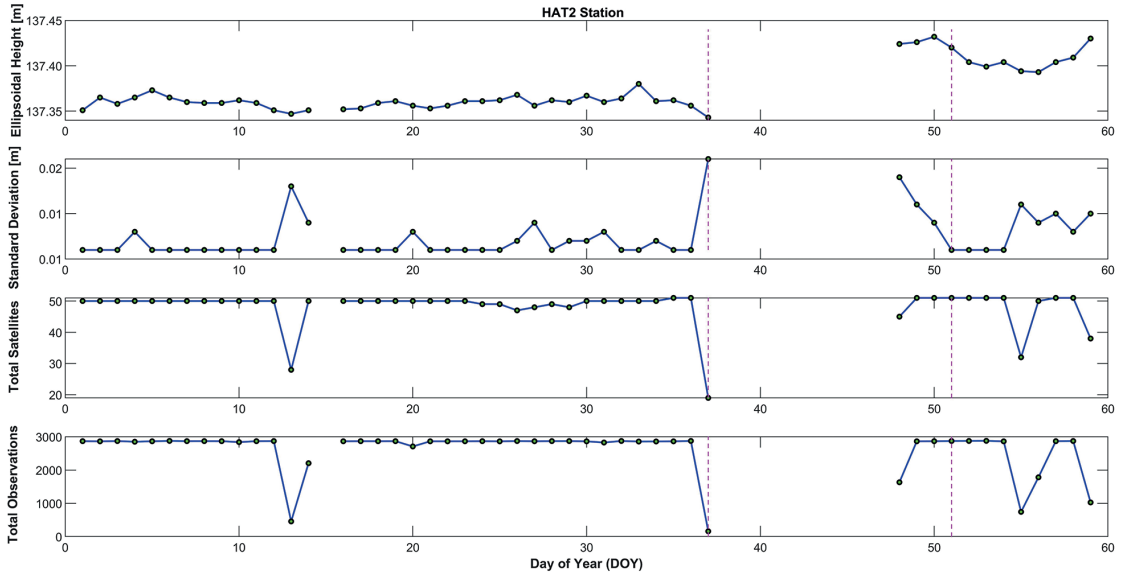

Fig. 7 - HAT2 (TUSAGA Point) ellipsoidal height, StD, total satellite numbers, and total observations (between DOY: 1 and DOY: 59).

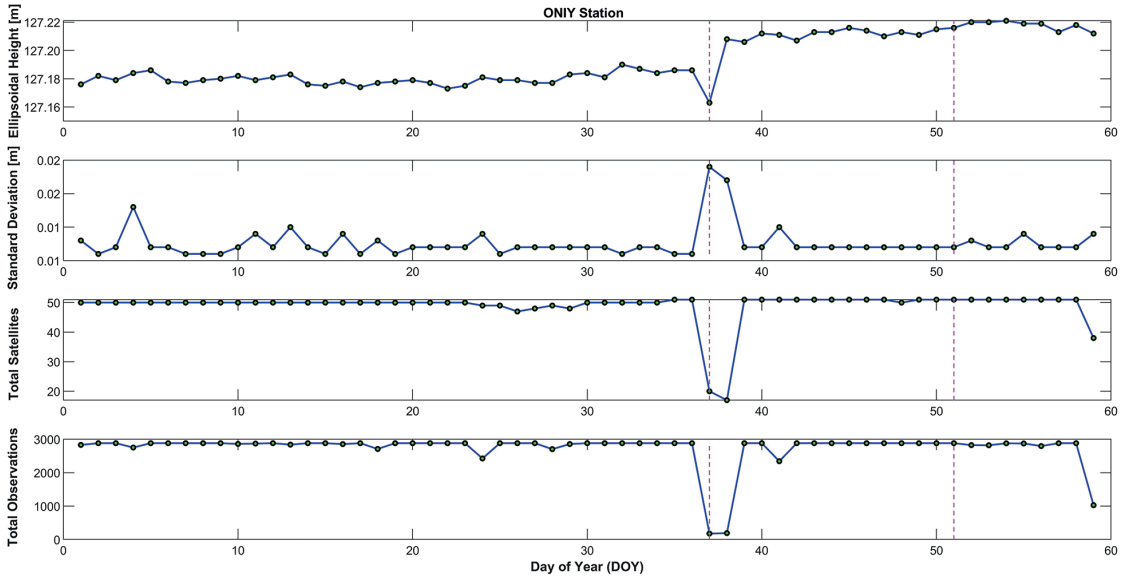

Fig. 8 - ONIY (TUSAGA Point) ellipsoidal height, StD, total satellite numbers, and total observations (between DOY: 1 and DOY: 59).

after the earthquake. This movement corresponds to an approximately 2-centimetre decrease, followed by a 4-centimetre increase. Therefore, it can be said that the height change movement at HAT2 and ONIY stations are similar.

The two GNSS points (HAT2 and ONIY) of the region can be seen in ellipsoidal height differences in different directions over time in Figs. 7 and 8. To see the changes in ellipsoidal

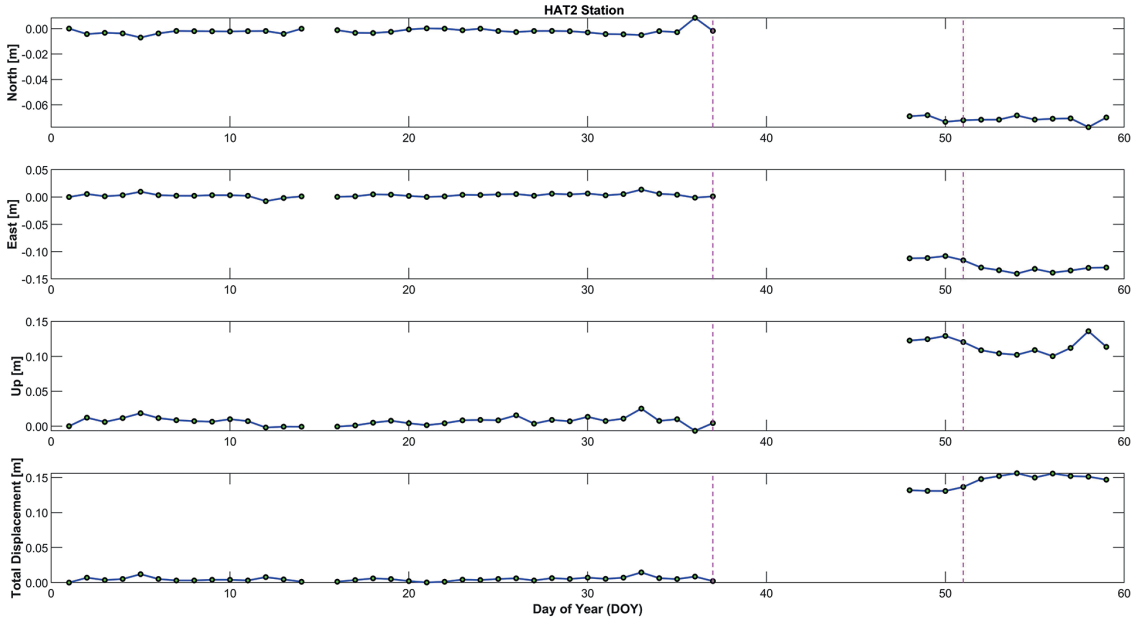

Fig. 9 - HAT2 (TUSAGA Point) N, E, and up values (between DOY: 1 and DOY: 59).

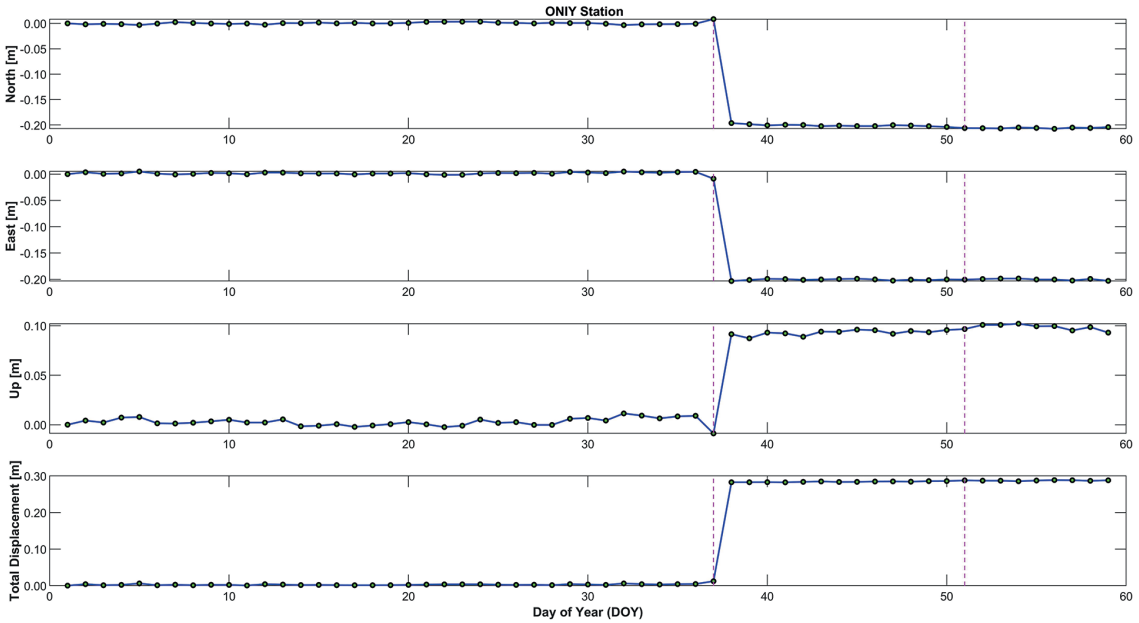

Fig. 10 - ONIY (TUSAGA point) N, E, and up values (between DOY: 1 and DOY: 59).

height more clearly, a N-E-up analysis of the GNSS points was also performed (Figs. 9 and 10). Up and ellipsoidal height represent the metric magnitude and direction of vertical movement. Fig. 9 illustrates the results of the analysis of horizontal movement (north and east) with precise point positioning (PPP). Following the earthquake on February 6, there was a movement of 13.4 cm; following the earthquake on 20 February, there was approximately 2.5 cm of movement. Furthermore, following the earthquakes on 6 and 20 February, the ONIY station showed a horizontal resultant movement of roughly 20 cm and one of less than 1 cm, respectively (Fig. 10). The metre-sized horizontal movements, which are one of the first findings of the earthquake and represent the plate movements (which caused outrage among people due to media coverage), cannot actually be detected at metre level since they are studied relatively and regionally with the remote sensing technique. Therefore, it is feasible to conclude that this research study yields more effective and reliable results when vertical movement is recorded appropriately for short-term InSAR monitoring.

This study monitored interferograms obtained from short-term data (see Figs. 11 and 12) and showed ground movements determined by fringes. In the literature, studies on the results obtained when ascending and descending orbit data sets are combined are generally conducted to show horizontal movements. This study found descending orbit data sufficient to show ground movements. In addition, since the devastating earthquakes of 6 and 20 February occurred very quickly, it was not necessary to make an additional time series to determine the deformation. Long-term deformation determination techniques such as the Small Baseline Subset or Permanent Scatterers Interferometric SAR techniques cannot produce the same results as rapidly as the DInSAR technique. Therefore, short-term DInSAR analysis is the best option for this study.

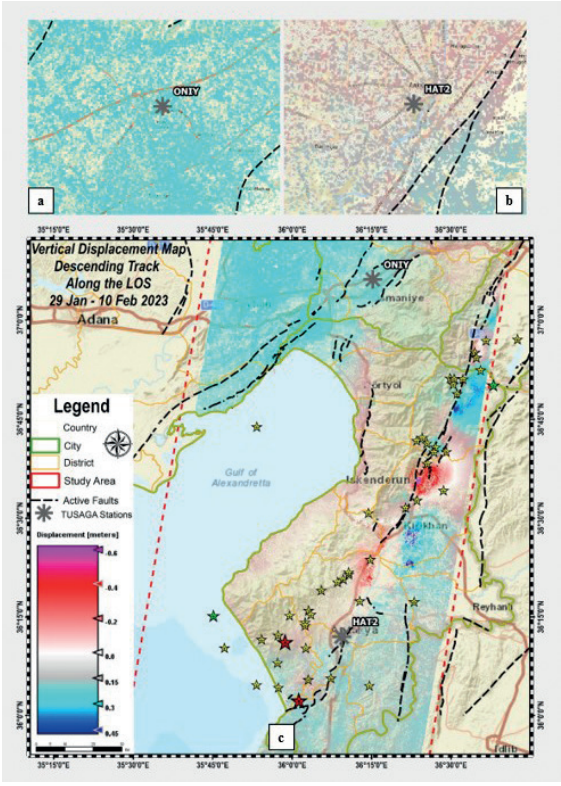

Fig. 11 - The map shows the ONIY TUSAGA point coseismic displacement (a); the HAT2 TUSAGA point coseismic displacement (b); and the coseismic map covers 29 January 2023 to 10 February 2023 (c).

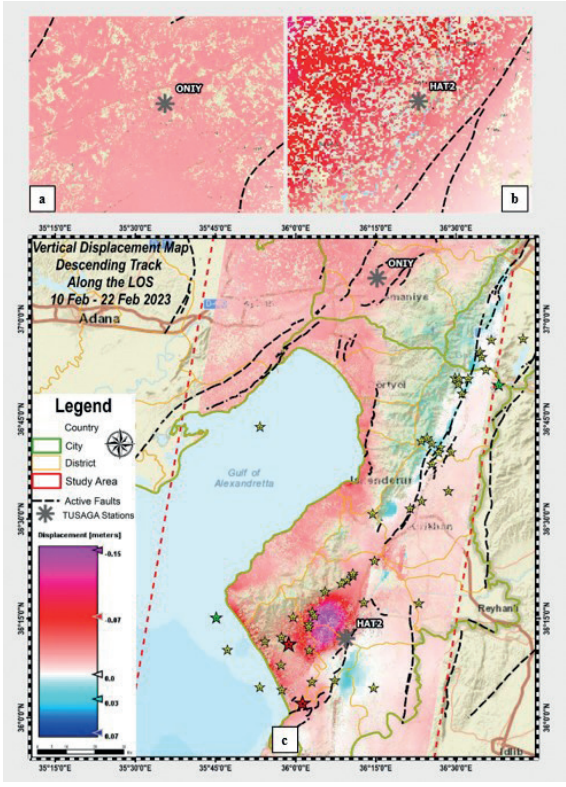

Fig. 12 - The map shows ONIY TUSAGA point coseismic displacement (a); HAT2 TUSAGA point coseismic displacement (b); the coseismic map covers 10 to 22 February 2023 (c).

4. Conclusions

In-situ studies cannot provide rapid and accurate results for determining surface deformations (especially mass movement) in large areas affected by devastating earthquakes. For this reason, vertical deformations can be determined by producing a displacement map using a remote sensing technique. With this scope, the earthquakes on 6 and 20 February in Hatay city were monitored with surface deformation maps produced with the DInSAR method using short-term Sentinel-1 SAR data. Additionally, two-month data, between DOY: 1 (1 January 2023) and DOY: 59 (28 February 2023), of HAT2 and ONIY CORS-TR stations were estimated using the Trimble-RTX service.

As a result, both the displacement map produced by the DInSAR method and the ellipsoidal height trend analysis resulting from the evaluation of HAT2 and ONIY station data present harmonious movement at CORS-TR stations in the 6 and 20 February earthquakes.

On 6 February 2023, the Pazarcık earthquake caused approximately 1 m of vertical deformation. As a result of the bending of the fault in the Amanos segment part of the EAFZ, the area where the Taşoluk village is located subsided by 60 cm, while the area with the Yuvalı village was uplifted by 44 cm. In the region defined as the Serinyol segment, south of Kırıkhan, the fault was determined to have a dip-slip component and, accordingly, the east of the fault was uplifted by 44 cm while the west of the fault subsided by 30 cm.

After the 20 February 2023 Hatay earthquake, 15 cm of vertical deformation was observed. As a result of the earthquakes occurring on normal and oblique-slip normal faults in the Hatay region, 15 cm of subsidence was determined as well, and vertical deformations were observed in the coastal areas due to mass movements. It is also observed that the İskenderun region is subducted 12 cm after the Hatay earthquake.

When displacement maps containing two different periods are compared, it is determined that the mass movements in the region are caused by the earthquakes that occurred after 10 February 2023, especially the devastating earthquake that occurred on 20 February 2023, triggering these mass movements.

Acknowledgments. The data used in this research were provided free of charge by ESA. We would like to thank the General Directorate of Land Registry and Cadastre and General Directorate of Mapping of Turkey for providing the data used in this study. Also, we would like to thank the Trimble Centerpoint RTX Post-Processing Service for data processing. The GNSS data sets are provided by TUSAGA-Active (Türkiye Ulusal Sabit GNSS Ağı-Aktif) System Earthquake Datasets (https://www.tusaga-aktif.gov.tr/Web/DepremVerileri.aspx). The Sentinel-1 data sets are provided by ESA, (https://dataspace.copernicus.eu/).

REFERENCES

Abdelmeguid M., Zhao C., Yalcinkaya E., Gazetas G., Elbanna A. and Rosakis A.; 2023: *Dynamics of episodic supershear in the 2023 M7.8 Kahramanmaraş/Pazarcik earthquake, revealed by near-field records and computational modeling.* Commun. Earth Environ., 4, doi: 10.1038/s43247-023-01131-7.

AFAD; 2023: *Earthquake Catalog*. <deprem.afad.gov.tr/event-catalog>.

Akıncı A.C. and Ünlügenç U.C.; 2023: 6 *February 2023 Kahramanmaraş earthquakes: geological data from the field, implications and assessment for Adana City.* Cukurova Univ. J. Faculty Eng., 38, 553-569, doi: 10.21605/cukurovaumfd.1334155.

Aksoy E., Akgun E., Softa M., Kocbulut F., Sozbilir H., Tatar O. and Erol S.C.; 2023: *Effect on the Eastern Anatolian Fault Zone Erkenek and Pazarcik segments of the 6 February 2023 Pazarcik (Kahramanmaras) earthquake: observations from Celikhan-Golbasi (Adiyaman).* Turk Deprem Arastirma Dergisi, 5, 85-104, doi: 10.46464/tdad.1280408.

Alkan R.M.; 2019: *Cm-level high accurate point positioning with satellite-based GNSS correction service in dynamic applications.* J. Spatial Sci., 66, 351-359, doi: 10.1080/14498596.2019.1643795.

Alkan R.M., Erol S., İlçi V. and Ozulu İ.M.; 2020: *Comparative analysis of real-time kinematic and PPP techniques in dynamic environment.* Meas., 163, doi: 10.1016/j.measurement.2020.107995.

Allen C.R.; 1969: *Active faulting in northern Turkey.* California Institute of Technology, Seismological Laboratory, Pasadena, CA, USA, 10 pp.

Altunsu E., Güneş O., Öztürk S., Sorosh S., Sarı A. and Beeson S.T.; 2024: *Investigating the structural damage in Hatay province after Kahramanmaraş-Türkiye earthquake sequences.* Eng. Fail. Anal., 157, doi: 10.1016/j.engfailanal.2023.107857.

Andreasyan H.D.; 1964: *Polonyalı Simeon'un seyahatnâmesi (1608-1619).* Baha Matbaası, İstanbul, Turkey, doi: 10.26650/AB/AA14.2022.148, in Turkish.

Andreasyan H.D.; 1973: *XIV. ve XV. Yüzyıl Türk tarihine ait ufak kronolojiler ve kolofonlar.* Tarih Enstitüsü Dergisi, Edebiyat Fakültesi Matbaasi, Istanbul, Turkey, pp. 83-148, in Turkish.

Andreasyan H.D. and Dulaurier E.; 1987: *Urfalı Mateos vekayi-nâmesi (952-1136) ve Papaz Grigor'un zeyli (1136-1162).* Türk Tarih Kurumu Basımevi (ed), Ankara, Turkey, 411 pp., in Turkish.

Arpat E. and Şaroğlu F.; 1972: *The East Anatolian Fault System; thoughts on its development.* Bull. Miner. Res. Explor., 78, 44-50.

Basciftci F. and Bulbul S.; 2022: *Investigation of ionospheric TEC changes potentially related to Seferihisar-Izmir earthquake (30 October 2020, Mw 6.6)*. Bull. Geoph. Ocean., 63, 403-426, doi: 10.4430/bgo00394.

Baser T., Nawaz K., Chung A., Faysal S. and Numanoglu O.A.; 2023: *Ground movement patterns and shallow foundation performance in Iskenderun coastline during the 2023 Kahramanmaras earthquake sequence.* Earthquake Eng. Eng. Vibration, 22, 867-881, doi: 10.1007/s11803-023-2205-9.

Brandl M., Chen X., Drescher R., Glocker M., Landau H., Nardo A., Nitschke M., Salazar D., Seeger S., Weinbach U. and Zhang F.; 2014: *Advancing Trimble RTX technology by adding BeiDou and Galileo.* In: Proc. ESA European Navigation Conference (ENC2014), Rotterdam, The Netherlands, pp. 14-17.

Bulbul S., Gundogan T., Inal C., Basciftci F. and Yildirim O.; 2023: *Monitoring deformations caused by Pazarcık (Mw = 7.7) and Ekinözü (Mw = 7.6) earthquakes in Kahramanmaraş on 6 February 2023 with GNSS.* Eur. Phys. J. Plus, 138, doi: 10.1140/epjp/s13360-023-04759-8.

Caglayan A., Isik V., Saber R., Unal H. and Chitea F.; 2023: *Analysis of surface rupture patterns and fault offset variability associated with the 06 February 2023 Pazarcik (Kahramanmaras) earthquake (Mw 7.7) in Islahiye area, Türkiye.* In: Proc. Eurasia Geoscience Congress and Exhibition, Antalya, Turkey, pp. 19-24.

Çalışkan V.; 2008: *Human-induced wetland degradation: a case study of Lake Amik (southern Turkey).* In: Abstracs Balwois Conference on Water Observation and Information System for Decision Support, Ohrid, Republic of Macedonia, pp. 1-10.

Chen C.W. and Zebker H.A.; 2001: *Two-dimensional phase unwrapping with use of statistical models for cost functions in nonlinear optimization.* J. Opt. Soc. Am. A, 18, 338-351, doi: 10.1364/JOSAA.18.000338.

Emre Ö., Duman T.Y., Özalp S., Elmacı H., Olgun Ş. and Şaroğlu F.; 2013: *Active fault map of Turkey with an explanatory text 1:1,250,000 scale.* General Directorate of Mineral Research and Exploration, Ankara, Turkey, Special Publication Series, 30, ISBN: 978-605-5310-56-1.

Erkoç M.H. and Doğan U.; 2023: *Datum definition for geodetic vertical velocity field derived from GNSS observations: a case study in western and southern Turkey.* Bull. Geoph. Ocean., 64, 135-148, doi: 10.4430/bgo00412.

Erol S., Alkan R.M., Ozulu İ.M. and İlçi V.; 2020: *Performance analysis of real-time and post-mission kinematic precise point positioning in marine environments.* Geod. Geodyn., 11, 401-410, doi: 10.1016/j.geog.2020.09.002.

Fattahi H., Agram P. and Simons M.; 2017: *A network-based enhanced spectral diversity approach for TOPS time-series analysis.* IEEE Trans. Geosci. Remote Sens., 55, 777-786, doi: 10.1109/TGRS.2016.2614925.

Ferretti A., Monti-Guarnieri A., Prati C., Rocca F. and Massonet D.; 2007: *InSAR. Principles-Guidelines for SAR interferometry processing and interpretation.* ESA Publications, Noordwijk, The Netherlands, TM-19, 252 pp.

Fusco A., Buonanno S., Zeni G., Monterroso F., Atzori S., Bordogna G., Carrara P., Bonano M., Zinno I. and Onorato G.; 2023: *A CNN-Based interferogram filtering approach to enhance the co-seismic surface displacements identification by exploiting the EPOSAR DInSAR maps global archive.* In: Proc. IEEE Int. Geosci. Remote Sens. Symp. (IGARSS 2023), Pasadena, CA, USA, pp. 5230-5233, doi: 10.1109/IGARSS52108.2023.10282743.

General Directorate of Mapping; 2018a: *TUSAGA-Active (Türkiye Ulusal Sabit GNSS Ağı-Aktif) System.* <www.harita.gov.tr/jeo/tusagaAktif.php>, accessed 1 December 2023, in Turkish.

General Directorate of Mapping; 2018b: *TUSAGA-Active (Türkiye Ulusal Sabit GNSS Ağı-Aktif) System Earthquake Dataset.* <www.tusaga-aktif.gov.tr/Web/DepremVerileri.aspx>, accessed 1 December 2023, in Turkish.

Goldstein R.M. and Werner C.L.; 1998: *Radar interferogram filtering for geophysical applications.* Geophys. Res. Lett., 25, 4035-4038, doi: 10.1029/1998GL900033.

Görüm T., Tanyas H., Karabacak F., Yılmaz A., Girgin S., Allstadt K.E., Süzen M.L. and Burgi P.; 2023: *Preliminary documentation of coseismic ground failure triggered by the February 6, 2023 Türkiye earthquake sequence.* Eng. Geol., 327, doi: 10.1016/j.enggeo.2023.107315.

Gupta A., Asopa U. and Bhattacharjee R.; 2019: *Land subsidence monitoring in Jagadhri City using Sentinel 1 data and DInSAR processing.* In: 2nd International Electronic Conference on Geosciences, MDPI Proceedings 2019, 24, 25, doi: 10.3390/IECG2019-06230.

Harzali M., Medhioub E., Abdelmalak M.M., Hamdouni A. and Troudi H.; 2023: *Insights from the 06 February 2023 Mw 7.8 Kahramanmaras earthquake: evidence into an active strike-slip faulting along the East Anatolian Fault Zone.* Acta Geod. Geophys., 58, 465-497, doi: 10.1007/s40328-023-00428-5.

Karabacak V., Özkaymak Ç., Sözbilir H., Tatar O., Aktuğ B., Özdağ Ö.C., Çakir R., Aksoy E., Koçbulut F. and Softa M.; 2023: *The 2023 Pazarcık (Kahramanmaraş, Türkiye) earthquake (Mw 7.7): implications for surface rupture dynamics along the East Anatolian Fault Zone*. J. Geol. Soc., 180, doi: 10.1144/jgs2023-020.

Kim T. and Han H.; 2023: *Coseismic displacement fields and the slip mechanism of the 2021 Mw 6.7 Hovsgol earthquake in Mongolia constrained by Sentinel-1 and ALOS-2 InSAR.* GISci. Remote Sens., 60, doi: 10.1080/15481603.2023.2180026.

Kobayashi T., Munekane H., Kuwahara M. and Furui H.; 2024: *Insights on the 2023 Kahramanmaraş Earthquake, Turkey, from InSAR: fault locations, rupture styles and induced deformation.* Geophys. J. Int., 236, 1068-1088, doi: 10.1093/gji/ggad464.

Krishnakumar V., Qiu Z., Monserrat O., Barra A., López-Vinielles J., Reyes-Carmona C., Gao Q., Cuevas-González M., Palamà R., Crippa B. and Gili J.A.; 2021: *Sentinel-1 A-DInSAR approaches to map and monitor ground displacements.* Remote Sens., 13, doi: 10.3390/rs13061120.

Kürçer A., Elmacı H., Özdemir E., Güven C., Güler T., Avcu İ., Olgun Ş., Avcı H.O., Aydoğan H., Yüce A.A., Çetin F.E., Ayrancı A., Akyol Z., Soykasap Ö.A., Altuntaş G., Demirörs U., Karayazı O., Bayrak A. and Özalp S.; 2023: *06 Şubat 2023 Pazarcık (Kahramanmaraş) Depremi (Mw 7,7) Saha Gözlemleri ve Değerlendirmele.* MTA Genel Müdürlüğü, Ankara, Turkey, Rapor no. 14138, 187 pp., <www.mta.gov.tr/v3.0/sayfalar/bilgi-merkezi/deprem/pdf/14138.pdf>, in Turkish.

Kwiatek G., Martínez-Garzón P., Becker D., Dresen G., Cotton F., Beroza G.C., Acarel D., Ergintav S. and Bohnhoff M.; 2023: *Months-long seismicity transients preceding the 2023 Mw 7.8 Kahramanmaraş earthquake, Türkiye.* Nat. Commun., 14, doi: 10.1038/s41467-023-42419-8.

Liu J., Li X., Nobile A., Klinger Y. and Jónsson S.; 2023: *Fault slip and fault-zone damage of the 6 February 2023 Kahramanmaraş earthquake duplet estimated from 3D displacement derivations of Sentinel-1 radar images*. In: Abstract EGU General Assembly, Copernicus Meetings, Vienna, Austria, doi: 10.5194/egusphere-egu23-17611.

Makineci H.B.; 2023: *Comparative accuracy analysis of DEMs generated from descending and ascending orbit TerraSAR-X data.* Bull. Geoph. Ocean., 64, 259-278, doi: 10.4430/bgo00427.

McClusky S., Balassanian S., Barka A., Demir C., Ergintav S., Georgiev I., Gurkan O., Hamburger M., Hurst K., Kahle H., Kastens K., Kekelidze G., King R., Kotzev V., Lenk O., Mahmoud S., Mishin A., Nadariya M., Ouzounis A., Paradissis D., Peter Y., Prilepin M., Reilinger R., Sanli I., Seeger H., Tealeb A., Toksöz M.N. and Veis G.; 2000: *Global Positioning System constraints on plate kinematics and dynamics in the eastern Mediterranean and Caucasus.* J. Geophys. Res.: Solid Earth, 105, 5695-5719, doi: 10.1029/1999JB900351.

Monterroso F., De Luca C., Bonano M., Lanari R., Manunta M., Manzo M., Zinno I. and Casu F.; 2018: *Automatic generation of co-seismic displacement maps by using Sentinel-1 interferometric SAR data.* Procedia Comput. Sci., 138, 332-337, doi: 10.1016/j.procs.2018.10.047.

Pawluszek-Filipiak K. and Borkowski A.; 2020: *Integration of DInSAR and SBAS techniques to determine mining-related deformations using Sentinel-1 data: the case study of Rydułtowy mine in Poland*. Remote Sens., 12, doi: 10.3390/rs12020242.

Rafiei F., Gharechelou S., Golian S. and Johnson B.A.; 2022: *Aquifer and land subsidence interaction assessment using Sentinel-1 data and DInSAR technique*. ISPRS Int. J. Geo-Inf., 11, doi: 10.3390/ijgi11090495.

Reilinger R., McClusky S., Vernant P., Lawrence S., Ergintav S., Cakmak R., Ozener H., Kadirov F., Guliev I., Stepanyan R., Nadariya M., Hahubia G., Mahmoud S., Sakr K., ArRajehi A., Paradissis D., Al-Aydrus A., Prilepin M., Guseva T., Evren E., Dmitrotsa A., Filikov S.V., Gomez F., Al-Ghazzi R. and Karam G.; 2006: *GPS constraints on continental deformation in the Africa-Arabia-Eurasia continental collision zone and implications for the dynamics of plate interactions.* J. Geophys. Res.: Solid Earth, 111, doi: 10.1029/2005JB004051.

Sandron D., Rebez A., Tamaro A. and Slejko D.; 2023: *Recent earthquakes (2000-2021) in and around the Friuli Venezia Giulia region (NE Italy) and quality improvements of the OGS network monitoring capabilities.* Bull. Geoph. Ocean., 64, 237-258, doi: 10.4430/bgo00421.

Sarmin F.J., Zaman M.S.U. and Sarkar A.R.; 2020: *Monitoring land deformation due to groundwater extraction using Sentinel-1 satellite images: a case study from Chapai Nawabgonj, Bangladesh.* In: Proc. 23rd International Conference on Computer and Information Technology (ICCIT), Dhaka, Bangladesh, pp. 1-6, doi: 10.1109/ICCIT51783.2020.9392684.

Şengör A.M.C.; 1980: *Türkiye'nin neotektoniğinin esasları.* Türkiye Jeoloji Kurumu yayını, Konferans Serisi 2, Ankara, Turkey, pp. 40, in Turkish.

Şengör A.M.C., Görür N. and Şaroğlu F.; 1985: *Strike-slip faulting and related basin formation in zones of tectonic escape: Turkey as a case study.* In: Biddle K.T. and Chrisite-Blick N. (eds), Strike-slip Deformation, Basin Formation, and Sedimentation, Society of Economic Paleontologists and Mineralogists, Tulsa, TX, USA, Special Publication, Vol. 37, pp. 227-264, doi: 102110/pec.85.37.0211.

Small D. and Schubert A.; 2019: *Guide to Sentinel-1 geocoding.* Remote Sensing Lab. Univ. Zurich (RSL), Zürich, Switzerland, Tech. Rep. UZHS1-GC-AD, 42 pp., <zsentinel.esa.int/documents/247904/1653442/Guide-to-Sentinel-1-Geocoding.pdf>.

Sonkar A., Kumar S. and Kumar N.; 2023: *Spaceborne SAR-Based detection of ships in Suez Gulf to analyze the maritime traffic jam caused due to the blockage of Egypt's Suez Canal.* Sustainability, 15, doi: 10.3390/su15129706.

Soysal H., Sipahioğlu S., Kolçak D. and Altinok Y.; 1981: *Historical earthquakes catalogue of Turkey and surrounding area (2100 BC-1900 AD).* The Scientific and Technical Research Council of Turkey (TUBİTAK), Ankara, Turkey, Project no. TBAG 341, Final report, 86 pp., in Turkish.

Trimble-RTX; 2021: *Trimble CenterPoint RTX Post-Processing Service.* <www.trimblertx.com/>.

Ullo S.L., Addabbo P., Di Martire D., Sica S., Fiscante N., Cicala L. and Angelino C.V.; 2019: *Application of DInSAR technique to high coherence Sentinel-1 images for dam monitoring and result validation through in situ measurements.* IEEE J. Sel. Top. Appl. Earth Obs. Remote Sens., 12, 875-890, doi: 10.1109/JSTARS.2019.2896989.

Xu L., Chen Q., Zhao J.-J., Liu X.-W., Xu Q. and Yang Y.-H.; 2021: *An integrated approach for mapping three-dimensional coseismic displacement fields from Sentinel-1 TOPS data based on DInSAR, POT, MAI and BOI techniques: application to the 2021 Mw 7.4 Maduo earthquake.* Remote Sens., 13, doi: 10.3390/rs13234847.

Yagüe-Martínez N., Prats-Iraola P., Gonzalez F.R., Brcic R., Shau R., Geudtner D., Eineder M. and Bamler R.; 2016: *Interferometric processing of Sentinel-1 TOPS data.* IEEE Trans. Geosci. Remote Sens., 54, 2220-2234, doi: 10.1109/TGRS.2015.2497902.

Yigit C.O., Bezcioglu M., Ilci V., Ozulu I.M., Alkan R.M., Dindar A.A. and Karadeniz B.; 2022: *Assessment of real-time PPP with Trimble RTX correction service for real-time dynamic displacement monitoring based on high-rate GNSS observations.* Meas., 201, doi: 10.1016/j.measurement.2022.111704.

Yildirim O., Yaprak S. and Inal C.; 2013: *Determination of 2011 Van/Turkey earthquake (M = 7.2) effects from measurements of CORS-TR network.* Geomatics, Natural Hazards and Risk, 5, 132-144, doi: 10.1080/19475705.2013.789453.

Zhang F., Brandl M., Chen X., Drescher R., Glocker M., Landau H., Leandro R., Nitschke M., Salazar D. and Weinbach U.; 2013: *Trimble CenterPoint RTX - a first study on supporting Galileo.* In: Proc. The European Navigation Conference, Vienna, Austria, 8 pp.

Zhang Y., Tang X., Liu D., Taymaz T., Eken T., Guo R., Zheng Y., Wang J. and Sun H.; 2023: *Geometric controls on cascading rupture of the 2023 Kahramanmaraş earthquake doublet.* Nat. Geosci., 16, 1054-1060, doi: 10.1038/s41561-023-01283-3.

Corresponding author: Hasan Bilgehan Makineci
Geomatics Engineering Department, Konya Technical University
Yeni Istanbul Street, Selçuklu, Konya, Turkey
Phone: +90 332 205 1640; e-mail: hbmakineci@ktun.edu.tr